

AUV Navigation Based on Inertial Navigation and Acoustic Positioning Systems

Lingxiao Wang

DEPT. OF ELECTRICAL, COMPUTER,
SOFTWARE AND SYSTEMS ENG.
Embry-Riddle Aeronautical University
Daytona Beach, FL, 32114.
lingxiaw@my.erau.edu

Shuo Pang

DEPT. OF ELECTRICAL, COMPUTER,
SOFTWARE AND SYSTEMS ENG.
Embry-Riddle Aeronautical University
Daytona Beach, FL, 32114.
pang2d8@erau.edu

Abstract—This paper presents implementations based on an extended Kalman filter (EKF) and an unscented Kalman filter (UKF) for navigation of an autonomous underwater vehicle (AUV). Maintaining an accurate localization of an AUV is difficult because radio frequency signals, such as the global position system (GPS) signals, are highly attenuated by water. To address this problem, this paper proposes a new navigation method based on an inertial navigation system (INS) aided by a Doppler velocity log (DVL) and a short baseline (SBL). The presented EKF and UKF fuse the information from sensors to produce an accurate estimate of positions. Results from simulations yield that EKF and UKF based navigation methods have the similar performance and navigation accuracy. The proposed navigation method has been experimentally validated using the navigation data acquired from simulations and water tests.

Index Terms—AUV navigation, Inertial navigation, EKF, UKF, Sensor data fusion, Acoustic positioning system

I. INTRODUCTION

In recent years, autonomous underwater vehicles (AUVs) have demonstrated versatile capabilities to conduct different marine survey missions. The design and implementation of navigation systems stand out as one of the most critical steps towards the successful operation of AUVs. Modern AUV navigation techniques fall into three main categories, namely inertial navigation system (INS) based methods, acoustic positioning systems, and geophysical navigation methods [1].

A. Inertial Navigation System

The INS based navigation methods are accurate within a short-term period. Due to their simple algorithms, these methods are the most common solution for AUV navigation [2]. In the INS based algorithms, a vehicle is given an initial position before performing navigation, and measurements from inertial measurement units (IMUs) including sensed accelerations and angular rates are integrated to calculate position and orientation. However, the position error in an INS based method is accumulated over time without boundaries [3] [4]. As a result, INS based methods are limited for short-range navigation missions. Another problem is the unknown initial position. Since the INS based methods can only estimate how far a vehicle has traveled but not where a vehicle is, the knowledge of the initial position is mandatory. One of possible solutions to limit the accumulated error is using sophisticated sensors

TABLE I
BASELINE LENGTH IN THREE PRIMARY TYPES OF ACOUSTIC POSITIONING SYSTEMS

	Baseline Length
Super Short Baseline	<10 centimeters
Short Baseline	20~50 meters
Long Baseline	100~6000+ meters

[5]. In addition, the use of external measurements, such as GPS modules [6], acoustic positioning systems [7] [8], compasses [9], and image sonars [10] is proved to be valid methods to aid the traditional INS based method and limit position error growth.

B. Acoustic Positioning System

In acoustic navigation techniques, localization is achieved by measuring ranges from the time of flight (TOF) of acoustic signals. Since acoustic signals have a lower absorption rate in the water as compared with radio frequency signals, they can propagate a longer distance in the water, which makes AUV navigation possible. There are three different types of acoustic positioning systems: short baseline (SBL) [11], super short baseline (SSBL) [12] or ultra-short baseline (USBL) [13], and long baseline (LBL) [14]. The word 'baseline' refers to the imaginary line connecting two transducers. Typically, an acoustic system has at least three transducers and one transponder.

The principal difference among these methods is the length of baseline [15]. Table I shows the length of baseline for different acoustic positioning systems. In the USBL acoustic positioning system, the length of baseline is smaller than 10 centimeters, and the transducers are closely spaced with a specific order on the baseline. In a SBL acoustic positioning system, the length of baseline is around 20 meters, and transducers are placed at opposite ends of a ship's hull. In a LBL acoustic positioning system, the length of baseline is over 100 meters. Thus, transducers are placed over a wide area on the sea floor.

Different types of acoustic positioning systems are deployed for different missions. For instance, USBL and SBL are more suitable for a short-range navigation and tracking mission, and

LBL is a more common solution for a long-range mission. Factors that reduce the performance of an acoustic positioning system include variations in the acoustic signal's velocity, environmental noises, the multi-path phenomenon caused by redundant reflections of acoustic signals, and the inhomogeneity of water.

C. Geophysical Navigation

Geophysical navigation is achieved by measuring geophysical parameters as references to obtain estimated positions of an AUV. Geophysical information such as bathymetries [16] [17] and anomalies in magnetic fields [18] are often used as references for AUV navigation. This navigation method is either by supplying an AUV with an existing map of the navigation area or by constructing a map over the course of the mission. When an AUV has a match of a geophysical feature, then it knows its location on the map. Sensors to detect environment features include cameras, imaging sonar, ranging sonar, and magnetometers. However, a high-quality map may be unavailable in the operating area before the navigation mission. Simultaneous localization and mapping (SLAM) techniques have been used on AUV navigation by using sonar [19] and image measurements [20] to construct or update a map. A key requirement for the SLAM is to extract and match features from measurements obtained from sensors, and extracted information can be used to limit the error growth in INS based methods.

D. Filtering and Estimation

The current generation of AUVs are equipped with multiple sensors that can make use of a combination of different measurements during a single mission to improve the navigation accuracy. To obtain an optimal estimation of an AUV position, a filter is a necessary method to combine measurements throughout a mission. The extended Kalman filter (EKF), based on the first-order linearization, is the most common method to estimate the unknown state due to its simplicity and light computational complexity. To improve the estimation accuracy of EKF, many other non-linear filters have been proposed such as unscented Kalman filter (UKF) [21] and particle filter (PF) [22] [23]. The performance of above localization algorithms depends largely on knowledge of the covariance of observation noise (R) and the covariance of the process noise (Q). Adaptive Kalman filter (AKF) [24] is an effective method to solve this problem. In the AKF based algorithm, Q and R are adaptively updated.

II. METHODOLOGIES

A. Project Description

The 'YellowFin' AUV was designed and built by the Robotics Association at the Embry-Riddle Aeronautical University for the 'RoboSub' AUV international competition. In the competition, competitors are required to build AUVs which can perform different underwater tasks such as passing gates, picking balls, launching torpedoes, etc. To autonomously accomplish these missions, an accurate navigation system is

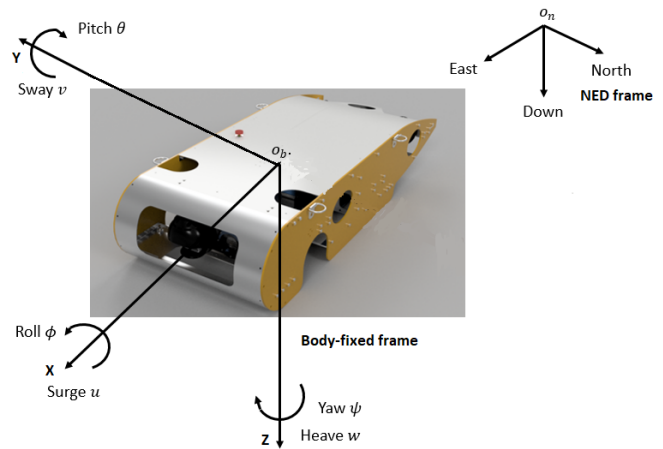


Fig. 1. The AUV in the body-fixed frame and the NED frame

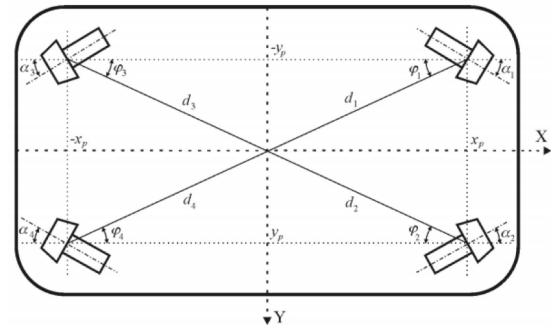


Fig. 2. The layout of four horizontal thrusters

necessary. Thus, the aim of our project is to design a valid navigation system.

Fig. 1 shows the 'YellowFin' AUV. The AUV was designed and manufactured to be streamlined and hydrodynamic, which can reduce the vertical lift and the horizontal drag when the AUV moves in water. Thanks to 7 thrusters from the Bluerobotics Inc., the AUV can be controlled in 6 degrees of freedom. Motions in surge, sway, and yaw are enabled by horizontal thrusters. Fig. 2 shows the layout of 4 horizontal thrusters. They were mounted in a vector configuration, and the angle between a thruster and the centerline is 45 degrees. Motions in roll, pitch, and heave are enabled by 3 vertical thrusters, two at the front and one at the back.

The sensor set available for the AUV includes:

- Inertial Measurement Unit (IMU);
- Depth Sensor;
- Doppler Velocity Log (DVL);
- Short Baseline (SBL).

B. Vehicle Modeling

To conveniently describe the AUV model, two suitable reference frames are used, shown in Fig. 1. The fixed inertial frame has its origin on the earth surface and its axes pointing to North, East, and Down (NED frame); the body-fixed frame

is centered in the center of gravity of the AUV, with the x-axis pointing in the forward direction, the y-axis pointing in the port direction, and the z-axis pointing down.

To describe the kinematic and the dynamic models of the vehicle, the society of naval architects and marine engineers (SNAME) notation [25] has been used. The model of an AUV is expressed in terms of the following vectors:

$$\boldsymbol{\eta} = [\boldsymbol{\eta}_1^T, \boldsymbol{\eta}_2^T]^T$$

$$\boldsymbol{\eta}_1 = [X, Y, Z]^T: \text{position in NED frame.}$$

$\boldsymbol{\eta}_2 = [\phi, \theta, \psi]^T$: orientation (Euler angles) describing the relation from the body-fixed frame to the NED frame.

$$\mathbf{v} = [\mathbf{v}_1^T, \mathbf{v}_2^T]^T$$

$$\mathbf{v}_1 = [u, v, w]^T: \text{linear velocities in body-fixed frame.}$$

$$\mathbf{v}_2 = [p, q, r]^T: \text{rotational velocities in body-fixed frame.}$$

The introduced quantities are linked by the following kinematic relation:

$$\dot{\boldsymbol{\eta}} = \mathbf{J}(\boldsymbol{\eta}_2)\mathbf{v}, \mathbf{J}(\boldsymbol{\eta}_2) = \begin{bmatrix} \mathbf{R}_b^N(\boldsymbol{\eta}_2) & \mathbf{0}_{3 \times 3} \\ \mathbf{0}_{3 \times 3} & \mathbf{T}_b^N(\boldsymbol{\eta}_2) \end{bmatrix}, \quad (1)$$

where $\mathbf{R}_b^N(\boldsymbol{\eta}_2)$ is the rotation between the NED frame and the body-fixed frame and $\mathbf{T}_b^N(\boldsymbol{\eta}_2)$ is the transformation matrix between angular velocity and the time derivatives of the Euler angles. They can be expressed as:

$$\mathbf{R}_b^N(\boldsymbol{\eta}_2) = \begin{bmatrix} c\psi c\theta & -s\psi c\phi + c\psi s\theta s\phi & s\psi s\phi + c\psi s\theta c\phi \\ s\psi c\theta & c\psi c\phi + s\psi s\theta s\phi & -c\psi s\phi + s\psi s\theta c\phi \\ -s\theta & c\theta s\phi & c\theta c\phi \end{bmatrix}, \quad (2)$$

$$\mathbf{T}_b^N(\boldsymbol{\eta}_2) = \begin{bmatrix} 1 & s\phi t\theta & c\phi t\theta \\ 0 & c\phi & -s\phi \\ 0 & s\phi/c\theta & c\phi/c\theta \end{bmatrix}, \quad (3)$$

where s , c , and t represent \sin , \cos , and \tan functions respectively.

The dynamics of the AUV is governed by the following equations [26]:

$$M\dot{\mathbf{v}} + C(\mathbf{v})\mathbf{v} + D(\mathbf{v})\mathbf{v} + \mathbf{g}(\boldsymbol{\eta}) = \boldsymbol{\tau}(\mathbf{v}, \mathbf{u}), \quad (4)$$

where M is the mass matrix, $C(\mathbf{v})$ and $D(\mathbf{v})$ are the centrifugal and Coriolis matrix and the damping effects matrix respectively, $\mathbf{g}(\boldsymbol{\eta})$ is the vector of gravitational and buoyancy effects, \mathbf{u} is the control inputs, and $\boldsymbol{\tau}(\mathbf{v}, \mathbf{u})$ is the vector of the resultant force and moment acting on the AUV.

C. The traditional INS Based Method

In the traditional INS based method, an IMU is sufficient to estimate position and orientation of an AUV. Estimated position and orientation are calculated by an integration of sensed accelerations and angular rates with given initial values of velocity, position, and orientation. Fig. 3 shows procedures of the traditional INS based method.

First of all, sensed angular rates (\mathbf{v}_2) measured from a gyroscope are transformed to time derivatives of the Euler angles ($\dot{\boldsymbol{\eta}}_2$) through the transformation (3), and results

from the transformation are integrated to be Euler angles ($\boldsymbol{\eta}_2$). Secondly, sensed accelerations ($\dot{\mathbf{v}}_1$) measured from an accelerometer are converted to accelerations in the NED frame ($\dot{\boldsymbol{\eta}}_1$) through the transformation (2), and results from the transformation are integrated to obtain velocities in the NED frame ($\boldsymbol{\eta}_1$). In the end, AUV position ($\boldsymbol{\eta}_1$) can be determined by the integration of velocities in the NED frame.

The traditional INS based method is a simple navigation method, which only needs an IMU as the measurement to obtain position and orientation. The disadvantage of the method is that errors are cumulative. Consequently, the error in the AUV position grows unbounded with distance traveled. To limit the error, a traditional INS based method is usually aided by other sensors that provide direct measurements of the integrated quantities. In the project, we aided the traditional INS based method by a DVL and a SBL, which can provide AUV velocity in the body-fixed frame and position in the NED frame respectively.

D. Navigation Filters

In order to use a recursive digital motion estimation filter (e.g. the Kalman filter), a discrete state-space representation of the vehicle model is needed. The system can be described by a set of equations in the form:

$$\begin{cases} \mathbf{x}_k = \mathbf{f}_{k-1}(\mathbf{x}_{k-1}, \mathbf{u}_{k-1}) + \mathbf{w}_{k-1} \\ \mathbf{y}_k = \mathbf{h}_k(\mathbf{x}_k) + \mathbf{v}_k \end{cases}, \quad (5)$$

where \mathbf{x}_k is the vector of state variables at the t_k time instant, \mathbf{u}_k and \mathbf{y}_k are the inputs and the outputs of the system, \mathbf{w}_k and \mathbf{v}_k are process and measurement noise, and $\mathbf{f}(\cdot)$ and $\mathbf{h}(\cdot)$ are prediction and observation models respectively. In this paper, the state vector \mathbf{x} has been chosen as the following vector:

$$\mathbf{x} = [X, Y, Z, u, v, w, \phi, \theta, \psi]. \quad (6)$$

The nonlinear AUV model indicates that a linear filter cannot be used to estimate system state. Thus, two nonlinear filters have been used, namely the Extended Kalman Filter (EKF) and the Unscented Kalman Filter (UKF). The EKF is the extended version of the Kalman Filter, which linearizes the nonlinear model about the current mean and covariance [27]. In the EKF's algorithm, there are two steps:

Algorithm 1. EKF algorithm

Step 1. Predict

Predicted state estimate:

$$\hat{\mathbf{x}}_k^- = \mathbf{f}_{k-1}(\hat{\mathbf{x}}_{k-1}^-, \mathbf{u}_k)$$

Predicted covariance estimate:

$$\mathbf{P}_k^- = \mathbf{F}_k \mathbf{P}_{k-1}^- \mathbf{F}_k^T + \mathbf{Q}_k$$

End

Step 2. Update

Near optimal Kalman Gain:

$$\mathbf{K}_k = \mathbf{P}_k^- \mathbf{H}_k^T (\mathbf{H}_k \mathbf{P}_k^- \mathbf{H}_k^T + \mathbf{R}_k)^{-1}$$

Updated state estimate:

$$\hat{\mathbf{x}}_k = \hat{\mathbf{x}}_k^- + \mathbf{K}_k (z_k - \mathbf{h}_k(\hat{\mathbf{x}}_k^-))$$

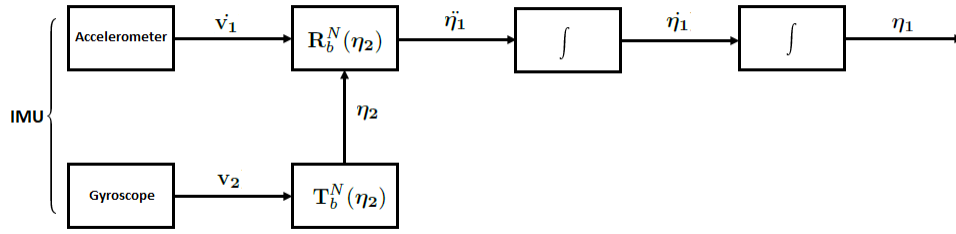


Fig. 3. Flow diagram of the traditional INS based method

Updated covariance estimate:

$$\mathbf{P}_k = (\mathbf{I} - \mathbf{K}_k \mathbf{H}_k) \mathbf{P}_k^-$$

End

In the EKF based algorithm, $\hat{\mathbf{x}}^-$ is the *a priori* state estimate, and $\hat{\mathbf{x}}$ is the *a posteriori* state estimate [27]. \mathbf{F}

and \mathbf{H} are the Jacobian forms of prediction and observation models. \mathbf{P} is the state covariance matrix. \mathbf{z} is the measurement vector. \mathbf{Q} and \mathbf{R} are the covariance matrices of process and observation noise respectively. At t_k time instant, states can be predicted based on estimates of the previous t_{k-1} time instant through the prediction model $\mathbf{f}(\mathbf{x}_k)$, and it is expressed in the discrete function as:

$$\mathbf{f}(\mathbf{x}_k) = \begin{bmatrix} X \\ Y \\ Z \\ u \\ v \\ w \\ \phi \\ \theta \\ \psi \end{bmatrix}_k = \begin{bmatrix} X_{k-1} + (u_{k-1} c \theta c \psi + v_{k-1} (s \phi s \theta c \psi - c \phi s \psi) + w_{k-1} (c \phi s \theta c \psi + s \phi s \psi)) T \\ Y_{k-1} + (u_{k-1} c \theta s \psi + v_{k-1} (s \phi s \theta s \psi + c \phi c \psi) + w_{k-1} (c \phi s \theta s \psi - s \phi c \psi)) T \\ Z_{k-1} + (-u_{k-1} s \theta + v_{k-1} s \phi c \theta + w_{k-1} c \phi c \theta) T \\ u_{k-1} + a_{xk-1} T \\ v_{k-1} + a_{yk-1} T \\ w_{k-1} + a_{zk-1} T \\ \phi_{k-1} + (p_{k-1} + q_{k-1} s \phi t \theta + r_{k-1} c \phi t \theta) T \\ \theta_{k-1} + (q_{k-1} c \phi - r_{k-1} s \phi) T \\ \psi_{k-1} + (q_{k-1} s \phi s e c \theta + r_{k-1} c \phi s e c \theta) T \end{bmatrix}, \quad (7)$$

where T is the sampling period.

In the prediction model, inputs are measured accelerations (\dot{u} , \dot{v} , \dot{w}) and angular rates (p , q , r) from the IMU. The measurement vector \mathbf{z} is defined as:

$$\mathbf{z}_k = [X, Y, Z, u, v, w, \phi, \theta, \psi]^T, \quad (8)$$

where, X , Y , and Z are measurement from the SBL, u , v , and w are provided by the DVL, and ϕ , θ , and ψ are provided by the IMU. All states are directly related to sensor measurements. Thus, the observation model at t_k time instant is expressed as:

$$\mathbf{h}_k(\mathbf{x}_k) = \mathbf{z}_k. \quad (9)$$

The flaw of the EKF based algorithm is the information lose in the linearization process. The approximation of a nonlinear function, however, can introduce errors in the EKF's estimations since the linearized model is no longer equal to the original model. Besides, the procedure to calculate Jacobian form of a nonlinear function is tedious and laborious. An alternative estimation technique is the unscented Kalman filter (UKF). In the UKF based algorithm, the state distribution is represented by a minimal set of carefully chosen sample points called sigma points. Sigma points are chosen so that their

mean and covariance to be exactly same with states' mean and covariance. Instead of propagating states in a linearized model like the EKF based algorithm, the UKF based algorithm propagates sigma positions through the original nonlinear model [28]. There are three steps in the UKF's algorithm:

Algorithm 2. UKF algorithm

Step 1. Calculate sigma points and weighting factors

$$\mathbf{X}_{k-1} = [\hat{\mathbf{x}}_{k-1}, \hat{\mathbf{x}}_{k-1} + \sqrt{(L + \lambda) \mathbf{P}_{k-1}}].$$

$$W_0^m = \lambda / (L + \lambda),$$

$$W_0^c = \lambda / (L + \lambda) + (1 - \alpha^2 + \beta),$$

$$W_i^m = W_i^c = 1 / (2(L + \lambda)), i = 1, 2, \dots, 2L,$$

End

Step 2. Time update

Propagate sigma points in the prediction model: $\mathbf{X}_k^- = \mathbf{f}(\mathbf{X}_{k-1}, \mathbf{u}_{k-1}), i = 0, 1, 2, \dots, 2L.$

$$\text{The mean of predicted state: } \hat{\mathbf{x}}_k^- = \sum_{i=0}^{2L} W_i^m \mathbf{X}_k^-.$$

$$\text{The covariance of predicted state: } \mathbf{P}_k^- = \sum_{i=0}^{2L} W_i^c (\mathbf{X}_k^- - \hat{\mathbf{x}}_k^-) (\mathbf{X}_k^- - \hat{\mathbf{x}}_k^-)^T + \mathbf{Q}_{k-1}.$$

Propagate sigma points in the observation model: $\varphi_k^- = \mathbf{h}(\mathbf{X}_k^-, \mathbf{u}_k).$

$$\text{The mean of predict output: } \hat{\mathbf{y}}_k^- = \sum_{i=0}^{2L} W_i^m \varphi_k^-.$$

End

Step 3. Measurement update

TABLE II
NOISE VARIANCES IN MEASURED VELOCITIES AND ACCELERATIONS

Measurements	Error Variance
u	4.46e-4
v	4.58e-4
w	1.05e-5
a_x	1.73e-4
a_y	1.39e-4
a_z	3.9e-4

The covariance of predict output: $\mathbf{P}_k^{yy} = \mathbf{R}_k + \sum_{i=0}^{2L} W_i^c (\boldsymbol{\varphi}_k^- - \hat{\mathbf{y}}_k^-) (\boldsymbol{\varphi}_k^- - \hat{\mathbf{y}}_k^-)^T$.

The cross-covariance between state and output: $\mathbf{P}_k^{xy} = \sum_{i=0}^{2L} W_i^c (\boldsymbol{\chi}_k^- - \hat{\mathbf{x}}_k^-) (\boldsymbol{\varphi}_k^- - \hat{\mathbf{y}}_k^-)^T$.

The Kalman gain: $\mathbf{K} = \mathbf{P}_k^{xy} (\mathbf{P}_k^{yy})^{-1}$.

Update state estimate: $\hat{\mathbf{x}}_k = \hat{\mathbf{x}}_k^- + \mathbf{K} (\mathbf{y}_k - \hat{\mathbf{y}}_k^-)$.

Update covariance estimate: $\mathbf{P}_k = \mathbf{P}_k^- - \mathbf{K} \mathbf{P}_k^{yy} \mathbf{K}^T$.

End

In the UKF based algorithm, $\boldsymbol{\chi}$ is the vector of sigma points. L is the size of the state vector. λ is the primary scaling parameter. \mathbf{P} is the state covariance. W^m and W^c are weighting factors. α determines the spread of sigma points around the mean of states. β is used to incorporate prior knowledge of the distribution of \mathbf{x} . φ is the propagation of sigma points in the observation model.

The state vector \mathbf{x} is the same with the EKF's algorithm. Therefore, L is 9. The prime scaling factor λ is defined as 1, and β is 2 for the Gaussian distribution. α is defined as a small positive value from 10^{-4} to 1, and we selected it as 10^{-3} . The prediction model $\mathbf{f}(\cdot)$ and observation model $\mathbf{h}(\cdot)$ in the UKF are the same models that we designed for the EKF.

III. EXPERIMENTS AND RESULTS

Experiments were designed and implemented to evaluate the proposed navigation methods. In simulations, we used the 'Matlab' software as the platform and designed an AUV simulator based on it. For water tests, the 'YellowFin' AUV was deployed in a swimming pool at the Embry-Riddle Aeronautical University. In this section, results from simulations and water tests are presented and analyzed.

A. Covariance Matrix of the Observation Noise

We designed and implemented an experiment to determine the covariance matrix of the observation noise in the EKF and UKF. In the experiment setup, the AUV was placed in a full water tank. Measurements from inertial sensors were recorded when the AUV was fully stationary. Around 105,000 measurements were recorded and were used to determine the covariance matrix of the observation noise. Table II shows variance of noise in velocities and accelerations. The variance of noise in position was calculated from the SBL. The SBL estimated the positioning error when a new measurement updated. Taking the square of the value, we considered the result as variance of the noise in position.

TABLE III
FUNCTIONS FOR THREE PATHS

	Sinusoidal	Circle	Straight
Position	$\mathbf{X} = t$ $\mathbf{Y} = A \sin(\omega t)$	$\mathbf{X} = A \cos(\omega t)$ $\mathbf{Y} = A \sin(\omega t)$	$\mathbf{X} = t$ $\mathbf{Y} = 1$
Velocity	$\dot{\mathbf{X}} = 1$ $\dot{\mathbf{Y}} = A \omega \cos(\omega t)$	$\dot{\mathbf{X}} = -A \omega \sin(\omega t)$ $\dot{\mathbf{Y}} = A \omega \cos(\omega t)$	$\dot{\mathbf{X}} = 1$ $\dot{\mathbf{Y}} = 0$
Acceleration	$\ddot{\mathbf{X}} = 0$ $\ddot{\mathbf{Y}} = -A \omega^2 \sin(\omega t)$	$\ddot{\mathbf{X}} = -A \omega^2 \cos(\omega t)$ $\ddot{\mathbf{Y}} = -A \omega^2 \sin(\omega t)$	$\ddot{\mathbf{X}} = 0$ $\ddot{\mathbf{Y}} = 0$
Orientation	$\phi = 0$ $\theta = 0$ $\psi = A \omega \cos(\omega t)$	$\phi = 0$ $\theta = 0$ $\psi = -\tan(\omega t)$	$\phi = 0$ $\theta = 0$ $\psi = 0$

B. Simulation Design

We have conducted a series of simulation experiments with different sensor combinations, their aim being to compare the accuracies of the EKF and UKF based navigation methods. The AUV was assumed to move three paths in simulations: the sinusoidal wave, the circle path, and the straight line. The AUV started from the point with coordinates (0,0) for the sinusoidal wave and the circle path and (0,1) for the straight path. The initial heading angle is 0 degrees and at a constant depth of 10 meters for three paths. As shown in table III, AUV position, velocity, acceleration, and orientation were governed by three groups of mathematical functions for three paths.

In table III, t is a discrete time series from 0 to 60 seconds with the sampling rate 0.1 seconds (600 points in total). The measurements from sensors were simulated by adding normally distributed random values with zero mean and standard deviation based on the calculated variance in section III-A to actual states. SBL measures positions in the NED frame. Therefore, measured positions from the SBL were simulated by adding errors directly to \mathbf{X} and \mathbf{Y} . Note that, DVL and IMU measure velocities and accelerations in the body-fixed frame. Thus, $\dot{\mathbf{X}}$, $\dot{\mathbf{Y}}$, $\ddot{\mathbf{X}}$, and $\ddot{\mathbf{Y}}$ need to be transferred from the NED frame to the body-fixed frame before adding random noise.

The updating rate of the SBL is not a constant, which varies from 0.1 seconds to 2 seconds depending on external environments. To simulate SBL's updating rate, we pick a random number from 0.1 seconds to 2 seconds as one time updating rate. The inertial sensors, IMU and DVL, have a fixed updating rate, which is 0.1 seconds in simulations. To synchronize updating rates between the SBL and inertial sensors, the SBL updates at 0.1 seconds, but the old SBL measurement will not change until a new measurement being updated.

Two sensor combinations were chosen in simulations:

- Configuration 1: AUV equipped with IMU and DVL
- Configuration 2: AUV equipped with IMU, DVL, and SBL

The first configuration is the DVL aided INS based navigation method (DVL/INS), and the second one is the proposed navigation method, which utilizes SBL and DVL aided INS based method (SBL+DVL/INS). Estimated states including

TABLE IV
MSES FOR POSITION IN TWO CONFIGURATIONS

		East		North	
		Config.1	Config.2	Config.1	Config.2
EKF	Sine wave	194.42	0.4410	0.4700	2.3405
	Circle path	20.971	0.4253	2.3818	0.2852
	Straight line	0.0659	0.4704	0.1242	0.0215
UKF	Sine wave	174.18	0.4633	0.4829	2.3414
	Circle path	21.667	0.4314	2.7862	0.2870
	Straight line	0.2606	0.4731	0.1256	0.022

position, velocity, and orientation were compared with actual states to evaluate performances of filters.

C. Simulation Results

Fig. 4 shows results of simulations based on the DVL/INS based navigation method. In these diagrams, the error between actual position and estimated position is increased over time. Especially in the sine path and the circle path, the position error is significant at the end point for either the EKF or the UKF. Since the AUV's heading does not change in the straight line, the position error is not obvious.

Fig. 5 shows results of simulations based on the configuration 2 (SBL+DVL/INS). Comparing with the first navigation method, the position error is reduced significantly in the sine path and the circle path. Estimated paths of two filters are very close to the actual paths. Particularly, the starting point overlaps with the end point in the circle path, which proves that the new navigation method had improved the accuracy of the DVL/INS based navigation method. In addition, the comparison between two filters (EKF and UKF), it is easily visible that both filters offered similar performance.

To mathematically evaluate the performance of the proposed navigation method, the mean square error (MSE) was calculated based on results of two navigation methods:

$$MSE = \frac{1}{N} \sum_{i=1}^N (x_i - \hat{x}_i)^2, \quad (10)$$

where N is the number of points (600 points).

MSE is the accumulated error between actual states and estimated states. Based on its definition, the small MSE means the tiny accumulated error and the better navigation accuracy. Table IV shows MSEs in position based on two configurations.

In most scenarios, values of MSE in the Config.2 (SBL+DVL/INS based method) are smaller than values in the Config.1 (DVL/INS based method). Particularly, in the sine path, the MSE of position based on the Config.1 is over 194.42 on the *East* and 0.47 on the *North* using the EKF algorithm. The UKF algorithm has similar MSEs: over 170 on the *East* and 0.48 on the *North*. Based on the Config.2, the MSE becomes 0.44 on the *East* and 2.34 on the *North* with the EKF algorithm and 0.46 on the *East* and 2.34 on the *North* with the UKF algorithm. Comparing with the Config.1, the MSE of position in the *East* is significantly reduced by using the SBL+DVL/INS based method. In addition, all MSEs

based on the Config.2 are smaller than 2.5, which yields a satisfactory navigation result.

Simulation results show that the proposed navigation method limits accumulated error in the INS based method, and it is feasible for the AUV navigation.

D. Water Tests

Water tests were conducted in a swimming pool at the Embry-Riddle Aeronautical University. The long edge of the pool was measured as 14.75 meters, and the short edge was measured as 6.2 meters. Three transducers from the SBL acoustic positioning system were placed at B_1 , B_2 , and B_3 forming a triangular shape as shown in Fig. 7. The distance between B_1 and B_2 is 3.3 meters, and the distance between B_1 and B_3 is 11.08 meters.

In water tests, the path of the AUV was a 'L' shape. To start with, the AUV moved along the long edge of the swimming pool until it reached the terminal. Next, the AUV made a 90 degrees turn and moved along the short edge until reaching the middle of the short edge. After that, the AUV made an 'U' turn and moved back to the start position following the same path it came.

Since a GPS module cannot work in water, and the AUV always moves along the swimming pool's walls in water tests, we used edges of the swimming pool as references and considered edges as the actual path of the AUV. To estimate position in water tests, we applied two navigation methods: DVL/INS and SBL+DVL/INS in water tests. The performances of two methods were compared and evaluated. Due to the similarity of EKF and UKF, only the EKF based algorithm was implemented to fuse sensor information in water tests.

Fig. 6 shows results of water tests. Three plots are presented in the diagram, and they are estimated path based on the DVL/INS based method (dotted line), the estimated path based on the proposed navigation method (solid line), and edges of the swimming pool (dashed line). In the diagram, two estimated paths were close to the expected path. However, the estimated path based on the DVL/INS based method had an obvious accumulated error between the starting point and the end point, which is 4.98m. After applying the new navigation method, this gap was reduced to be 1.25m. The results from the water tests reveal that the proposed navigation method improves the INS based method.

IV. CONCLUSION

This paper addressed the design of a navigation system for the AUV with two inertial sensors, the IMU and the DVL, and one external sensor, the SBL. The main contributions of the paper are the implementations of the EKF and UKF algorithms in the AUV navigation. The prediction model and the observation model were designed based on the AUV's kinematic equations and relationships between states and sensors' measurements. Two types of experiments, simulations and water tests, were conducted to evaluate the performance of the proposed navigation method. Results from experiments

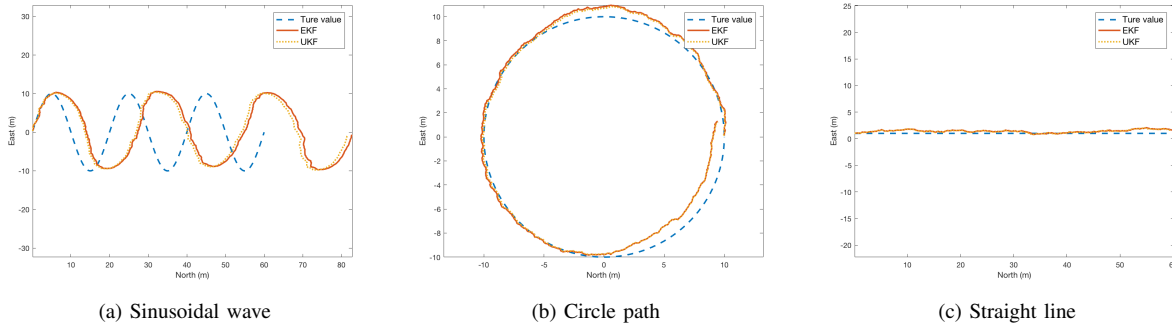


Fig. 4. Config.1: comparison between actual paths (dashed line) and estimated paths based on the DVL/INS method (solid line for the EKF based algorithm and dotted line for the UKF based algorithm)

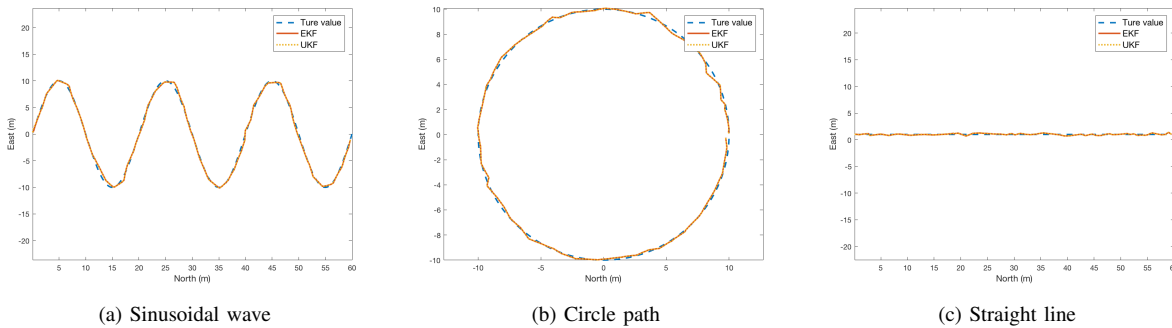


Fig. 5. Config.2: comparison between actual paths (dashed line) and estimated paths based on the SBL+DVL/INS method (solid line for the EKF based algorithm and dotted line for the UKF based algorithm)

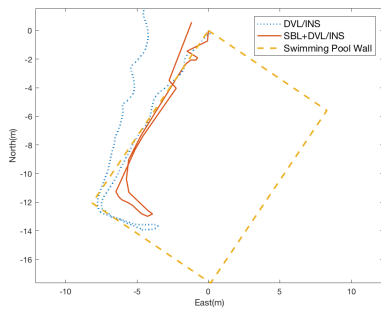


Fig. 6. Water test: comparison between the expected path (dashed line), the estimated path based on DVL/INS based method (dotted line), and the SBL+DVL/INS method (solid line)

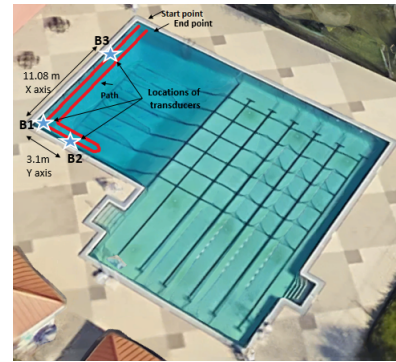


Fig. 7. The layout of transducers ($B1$, $B2$, and $B3$) network of the SBL and the expected path (red line) of the AUV

yield the validity of the proposed navigation method from two tests. The largest error found in simulation programs was around 0.80 and around 1.79 meters in water tests.

REFERENCES

- [1] L. Paull, S. Saeedi, M. Seto, and H. Li, "Auv navigation and localization: A review," *IEEE Journal of Oceanic Engineering*, vol. 39, no. 1, pp. 131–149, 2014.
- [2] M. Morgado, "Advanced ultra-short baseline inertial navigation systems," *UNIVERSIDADE TÉCNICA DE LISBOA INSTITUTO SUPERIOR TÉCNICO*, 2011.
- [3] O. J. Woodman, "An introduction to inertial navigation," University of Cambridge, Computer Laboratory, Tech. Rep., 2007.
- [4] Y. Huang, Y. Zhang, and X. Wang, "Kalman-filtering-based in-motion coarse alignment for odometer-aided sins," *IEEE Transactions on Instrumentation and Measurement*, vol. 66, no. 12, pp. 3364–3377, 2017.
- [5] R. Panish and M. Taylor, "Achieving high navigation accuracy using inertial navigation systems in autonomous underwater vehicles," in *OCEANS, 2011 IEEE-Spain*. IEEE, 2011, pp. 1–7.
- [6] M. F. Fallon, G. Papadopoulos, J. J. Leonard, and N. M. Patrikalakis, "Cooperative auv navigation using a single maneuvering surface craft," *The International Journal of Robotics Research*, vol. 29, no. 12, pp. 1461–1474, 2010.
- [7] D. J. Thomson, S. E. Dosso, and D. R. Barclay, "Modeling auv

- localization error in a long baseline acoustic positioning system,” *IEEE Journal of Oceanic Engineering*, 2017.
- [8] I. Burdinsky and S. Otcheskii, “Observation error estimation in case of an auv using a single beacon acoustic positioning system,” in *Integrated Navigation Systems (ICINS), 2017 24th Saint Petersburg International Conference on*. IEEE, 2017, pp. 1–4.
 - [9] Y. Zhu, X. Cheng, L. Wang, and L. Zhou, “An intelligent fault-tolerant strategy for auv integrated navigation systems,” in *Advanced Intelligent Mechatronics (AIM), 2015 IEEE International Conference on*. IEEE, 2015, pp. 269–274.
 - [10] P. Woock and C. Frey, “Deep-sea auv navigation using side-scan sonar images and slam,” in *OCEANS 2010 IEEE-Sydney*. IEEE, 2010, pp. 1–8.
 - [11] S. Smith and D. Kronen, “Experimental results of an inexpensive short baseline acoustic positioning system for auv navigation,” in *OCEANS’97. MTS/IEEE Conference Proceedings*, vol. 1. IEEE, 1997, pp. 714–720.
 - [12] R. Costanzi, N. Monnini, A. Ridolfi, B. Allotta, and A. Caiti, “On field experience on underwater acoustic localization through usbl modems,” in *OCEANS 2017-Aberdeen*. IEEE, 2017, pp. 1–5.
 - [13] D. Ribas, P. Ridaou, A. Mallios, and N. Palomeras, “Delayed state information filter for usbl-aided auv navigation,” in *Robotics and Automation (ICRA), 2012 IEEE International Conference on*. IEEE, 2012, pp. 4898–4903.
 - [14] M. V. Jakuba, C. N. Roman, H. Singh, C. Murphy, C. Kunz, C. Willis, T. Sato, and R. A. Sohn, “Long-baseline acoustic navigation for under-ice autonomous underwater vehicle operations,” *Journal of Field Robotics*, vol. 25, no. 11-12, pp. 861–879, 2008.
 - [15] K. Vickery, “Acoustic positioning systems. a practical overview of current systems,” in *Autonomous Underwater Vehicles, 1998. AUV’98. Proceedings of the 1998 Workshop on*. IEEE, 1998, pp. 5–17.
 - [16] S. Barkby, S. Williams, O. Pizarro, and M. Jakuba, “Incorporating prior maps with bathymetric distributed particle slam for improved auv navigation and mapping,” in *OCEANS 2009, MTS/IEEE Biloxi-Marine Technology for Our Future: Global and Local Challenges*. IEEE, 2009, pp. 1–7.
 - [17] O. Bergem, “A multibeam sonar based positioning system for an auv,” in *International symposium on unmanned untethered submersible technology*. University of New Hampshire-Marine Systems, 1993, pp. 291–291.
 - [18] C. Tyren, “Magnetic anomalies as a reference for ground-speed and map-matching navigation,” *The Journal of navigation*, vol. 35, no. 2, pp. 242–254, 1982.
 - [19] J. L. Leonard, R. N. Carpenter, and H. J. S. Feder, “Stochastic mapping using forward look sonar,” *Robotica*, vol. 19, no. 5, pp. 467–480, 2001.
 - [20] R. M. Eustice, “Large-area visually augmented navigation for autonomous underwater vehicles,” Ph.D. dissertation, Massachusetts Institute of Technology and Woods Hole Oceanographic Institution, 2005.
 - [21] B. Allotta, A. Caiti, R. Costanzi, F. Fanelli, D. Fenucci, E. Meli, and A. Ridolfi, “A new auv navigation system exploiting unscented kalman filter,” *Ocean Engineering*, vol. 113, pp. 121–132, 2016.
 - [22] G. T. Donovan, “Position error correction for an autonomous underwater vehicle inertial navigation system (ins) using a particle filter,” *IEEE Journal of Oceanic Engineering*, vol. 37, no. 3, pp. 431–445, 2012.
 - [23] S. Saeedi, M. Seto, and H. Li, “Fast monte carlo localization of auv using acoustic range measurement,” in *Electrical and Computer Engineering (CCECE), 2015 IEEE 28th Canadian Conference on*. IEEE, 2015, pp. 326–331.
 - [24] A. Mohamed and K. Schwarz, “Adaptive kalman filtering for ins/gps,” *Journal of geodesy*, vol. 73, no. 4, pp. 193–203, 1999.
 - [25] T. I. Fossen, “Marine control system-guidance, navigation and control of ships, rigs and underwater vehicles,” *Marine Cybernetics*, 2002.
 - [26] —, *Handbook of marine craft hydrodynamics and motion control*. John Wiley & Sons, 2011.
 - [27] G. Bishop, G. Welch *et al.*, “An introduction to the kalman filter,” *Proc of SIGGRAPH, Course*, vol. 8, no. 27599-3175, p. 59, 2001.
 - [28] E. A. Wan and R. Van Der Merwe, “The unscented kalman filter for nonlinear estimation,” in *Adaptive Systems for Signal Processing, Communications, and Control Symposium 2000. AS-SPCC. The IEEE 2000*. Ieee, 2000, pp. 153–158.